Published in final edited form as:
Neuroimage. 2014 February 1; 86: 244–256. doi:10.1016/j.neuroimage.2013.09.053.

Brain microstructural development at near-term age in very-low-birth-weight preterm infants: An atlas-based diffusion imaging study

Jessica Rose[a,b,*], **Rachel Vassar**[a], **Katelyn Cahill-Rowley**[b,c], **Ximena Stecher Guzman**[a], **David K. Stevenson**[e], and **Naama Barnea-Goraly**[f]

[a] Department of Orthopaedic Surgery, Stanford University School of Medicine, USA

[b] Motion Analysis Lab, Lucile Packard Children's Hospital, USA

[c]*Department of BioEngineering, Stanford, CA, USA*

[d] Radiology Department, Facultad de Medicina Clínica Alemana, Universidad del Desarrollo, Chile

[e] Division of Neonatology and Developmental Medicine, Stanford University School of Medicine, Stanford, CA, USA

[f] Center for Interdisciplinary Brain Sciences Research, Stanford University School of Medicine, USA

Abstract

At near-term age the brain undergoes rapid growth and development. Abnormalities identified during this period have been recognized as potential predictors of neurodevelopment in children born preterm. This study used diffusion tensor imaging (DTI) to examine white matter (WM) microstructure in very-low-birth-weight (VLBW) preterm infants to better understand regional WM developmental trajectories at near-term age.

DTI scans were analyzed in a cross-sectional sample of 45 VLBW preterm infants (BW ≤ 1500 g, GA ≤ 32 weeks) within a cohort of 102 neonates admitted to the NICU and recruited to participate prior to standard-of-care MRI, from 2010 to 2011, 66/102 also had DTI. For inclusion in this analysis, 45 infants had DTI, no evidence of brain abnormality on MRI, and were scanned at PMA ≤40 weeks (34.7–38.6). White matter microstructure was analyzed in 19 subcortical regions defined by DiffeoMap neonatal brain atlas, using threshold values of trace b0.006 mm^2 s^{-1} and FA >0.15. Regional fractional anisotropy (FA), mean diffusivity (MD), axial diffusivity (AD), and radial diffusivity (RD) were calculated and temporal–spatial trajectories of development were examined in relation to PMA and brain region location.

Posterior regions within the corona radiata (CR), corpus callosum (CC), and internal capsule (IC) demonstrated significantly higher mean FA values compared to anterior regions. Posterior regions of the CR and IC demonstrated significantly lower RD values compared to anterior regions. Centrally located projection fibers demonstrated higher mean FA and lower RD values than peripheral regions including the posterior limb of the internal capsule (PLIC), cerebral peduncle, retrolenticular part of the IC, posterior thalamic radiation, and sagittal stratum. Centrally located association fibers of the external capsule had higher FA and lower RD than the more peripherally-located superior longitudinal fasciculus (SLF). A significant relationship between PMA-at-scan

* Corresponding author at: 770 Welch Road, Suite 400, Stanford, CA 94304, USA. jessica.rose@stanford.edu (J. Rose)..

and FA, MD, and RD was demonstrated by a majority of regions, the strongest correlations were observed in the anterior limb of the internal capsule, a region undergoing early stages of myelination at near-term age, in which FA increased (r = .433, p = .003) and MD (r = –.545, p = .000) and RD (r = –.540, p = .000) decreased with PMA-at-scan. No correlation with PMA-at-scan was observed in the CC or SLF, regions that myelinate later in infancy.

Regional patterns of higher FA and lower RD were observed at this near-term age, suggestive of more advanced microstructural development in posterior compared to anterior regions within the CR, CC, and IC and in central compared to peripheral WM structures. Evidence of region-specific rates of microstructural development was observed. Temporal–spatial patterns of WM microstructure development at near-term age have important implications for interpretation of near-term DTI and for identification of aberrations in typical developmental trajectories that may signal future impairment.

Keywords

Diffusion tensor imaging; White matter microstructure; Brain development; Preterm neonates

Introduction

At near-term age, the brain undergoes rapid growth and microstructural development (Brody et al., 1987; Dubois et al., 2006; Huang et al., 2006; Kinney et al., 1988; Nossin-Manor et al., 2013; Oishi et al., 2011). Abnormalities identified during this period have been recognized as potential predictors of neurodevelopment in children born preterm (Aeby et al., 2013; Arzoumanian et al., 2003; Mukherjee et al., 2002; Rose et al., 2007, 2009; Thompson et al., 2012; van Kooij et al., 2011, 2012; Woodward et al., 2012). Advances in neonatal medicine have improved survival rates and outcome among preterm infants, however, 40–50% of very preterm infants experience neurodevelopmental impairments, including cerebral palsy, developmental coordination disorder, as well as cognitive and language delays (Spittle et al., 2011; Williams et al., 2010). At term-equivalent age, prematurity has been found to be associated with reduced cerebral volume and WM immaturity compared to term-born neonates (Hüppi et al., 1998; Inder et al., 2005; Lee et al., 2012; Rose et al., 2008; Thompson et al., 2006, 2013). However, little is known about the effect of timing, location, and severity of WM injury on neurodevelopment and future function. Near-term neuroimaging holds potential for establishing early biomarkers for future impairment to guide early intervention at a time of optimal neuroplasticity and rapid musculoskeletal growth.

Brain MRI is commonly assessed in very-low-birth-weight (VLBW) preterm infants prior to discharge from the NICU and offers an opportunity for early prognosis. To date, structural MRI has been only partially successful at detecting risk for neurodevelopmental problems later in life (Benini et al., 2012; Kidokoro et al., 2011). Diffusion tensor imaging (DTI) allows quantitative analysis of brain microstructure based on patterns of water diffusion (Basser and Pierpaoli, 1996; Counsell et al., 2002; Hüppi et al., 1998; Pierpaoli et al., 1996) and has shown promise for early prognosis of developmental outcome (Arzoumanian et al., 2003; Rose et al., 2007, 2009). As the brain develops, brain water content decreases, extracellular spaces diminish in size, and intra- and intercellular microstructures become more complex and organized. New barriers to water mobility form, such as axonal cell membranes, dendrites, and development of WM structural coherence and myelination that restrict water diffusion (Dubois et al., 2008; Kinney et al., 1994; Nossin-Manor et al., 2013). Scalars obtained from DTI can assess brain development and maturation and include fractional anisotropy (FA), mean diffusivity (MD), axial diffusivity (AD), and radial

diffusivity (RD) (Pierpaoli et al., 1996). FA reflects the degree of diffusion anisotropy within a voxel, and is determined by fiber diameter and density, myelination, extracellular diffusion, inter-axonal spacing, and intravoxel fiber-tract coherence. AD, a measure of diffusivity along the primary axis of diffusion within a voxel, is thought to reflect fiber coherence, and structure of axonal membranes (Song et al., 2002). RD, the mean of the diffusivities perpendicular to the primary axis of diffusion, is thought to represent degree of myelination (Chen et al., 2011; Song et al., 2002). MD is a calculation of average diffusion along the three main axes, relative to the primary direction of diffusion (AD). In neonates, FA has been found to increase, while MD, AD, and RD decrease, with age in WM regions, likely due to increased fiber organization, axonal coherence, and preliminary myelination (Aeby et al., 2009; Dubois et al., 2008; Mukherjee et al., 2002; Partridge et al., 2004; Shim et al., 2012).

Previous post-mortem and in-vivo fetal imaging studies in humans and histochemical imaging studies in animals suggest that early brain development follows an organized pattern (Bockhorst et al., 2008; Brody et al., 1987; Rajagopalan et al., 2012; Vasung et al., 2010; Yakovlev and Lecours, 1967; Yoshida et al., 2013). Specifically, postmortem anatomical study of human brain development at 12–22 weeks using 7.0 T MR identified the germinal matrix in the periventricular zone as early as 12 weeks GA (Meng et al., 2012). Huang et al. (2009) used DTI for post-mortem anatomical study of brain development from 13 to 22 weeks GA, and identified centrally located brainstem WM tracts, including the lower corticospinal tract (CST) and limbic fibers in the fornix and stria terminalis, at 13 weeks. During the second trimester, commissural, projection, and some association tracts were identified; the corpus callosum (CC) and internal capsule (IC) were visible at approximately 15 weeks. Association fibers of the sagittal stratum (SS) and external capsule (EC) were identified at 13–15 weeks. The cerebral peduncle (CereP) and IC developed earlier than more peripheral regions that extended into the corona radiata (CR) at 19–20 weeks (Huang et al., 2009).

As neurogenesis and neurodevelopment proceed, recently formed neurons migrate from the centrally-located germinal matrix to outer aspects of the cortical plate, producing the “inside out” order of cortical layers (Rakic, 1988). Cortical thickening and deepening of sulci continue during the second and third trimesters (Zhang et al., 2011, 2013) and the underlying intermediate zone matures into WM that contains afferent and efferent axons (Rakic, 1988). Proliferation and migration of oligodendrocytes, formed in centrally-located germinal matrix, ensheath axons and form myelin (Liu et al., 2013), influencing temporal–spatial patterns of WM development.

During the first two years of life, regional WM has been found to develop in a central-to-peripheral direction (Gao et al., 2008). Within specific regions such as the IC and CC, myelination has been reported to progress primarily from posterior-to-anterior direction with fronto-cortical brain regions the last to myelinate (Deoni et al., 2011; Geng et al., 2012; Kinney et al., 1988; Löbel et al., 2009; van der Knaap and Valk, 1990; Yoshida et al., 2013). DTI analysis of WM in full-term infants demonstrated progressive increase in FA and decrease in MD, AD, and RD with age (Gao et al., 2008; Geng et al., 2012; Yoshida et al., 2013).

In this study we use DTI to examine patterns of regional WM microstructure development in a cross-sectional sample of preterm infants with no evidence of brain injury on MRI, to better understand temporal–spatial trajectories of WM development at near-term age. Atlas-based DTI was used in order to quantify the developmental status of brain regions at near-term age, including WM microstructure and relative volume, using a semi-automated approach with potential clinical applications (Oishi et al., 2011, 2013). We hypothesized that

posterior regions within WM structures will show evidence of earlier microstructural development relative to anterior portions, and that centrally-located WM projection fibers will demonstrate evidence of earlier development than peripherally-located projection and association fibers.

Methods

Neonatal scans were obtained from 102 VLBW neonates, representing 76% of eligible participants admitted to Lucile Packard Children's Hospital (LPCH) and scanned between 1/1/10–12/31/11. Parents of all infants with GA ≤32 weeks, BW ≤1500 g, with no evidence of genetic disorders or congenital brain abnormalities were approached prior to scheduled standard-of-care MRI and consent was obtained for this IRB-approved study. Infants with no evidence of congenital brain abnormalities on MRI were included. 66 of 102 had successful DTI scans, collected at the end of the MRI scans, which are performed as standard-of-care at LPCH for all VLBW preterm infants at near-term age. 45 were scanned before 40 weeks PMA and had no evidence of brain abnormalities as reported by the clinical neuroradiologist and confirmed by a second neuroradiologist X.S.

MRI data acquisition

Brain MRI scans performed on 3T MRI (GE Discovery MR750, GE 8-Channel HD head coil) at LPCH, included T1, T2-weighted scans and diffusion-weighted scans (b = 1000 s/mm^2). The DTI was based on diffusion-weighted, single-shot, spin-echo, echo-planar imaging sequence of 25 directions, with slice thickness of 3 mm, matrix size of 128 × 128, and 90° flip angle. Two repetitions (~5 min each) were collected. Diffusion-weighted sequences were collected at the end of the ~25-minute standard-of-care MRI scan. Infants were swaddled and fed and typically remained asleep.

DTI processing

Diffusion-weighted images were pre-processed using DTI-Studio. The best repetition was selected to eliminate images with artifacts or evidence of motion for infants with at least two repetitions (n = 64/66). If no full repetition was usable a composite repetition was generated based on best image slices. An infant's DTI scan was included if at least one quality image was obtained for each slice from either repetition. Infants were excluded if neither repetition provided a viable image for any given slice or if it was not possible to combine the two repetitions due to orientation differences between the two repetitions, due to head movement between the two repetitions. Automated image registration was performed using an affine transformation to further correct for eddy current distortions and motion.

Each brain image was skull-stripped with ROI Editor using B0 and trace images to distinguish brain matter from intracranial CSF and skull, and manually rotated to align with the JHU neonatal template image. DTI images were processed with DiffeoMap (www.mristudio.org) using FA and trace maps to perform a large deformation diffeomorphic metric mapping (LDDMM) transformation (Oishi et al., 2011). Each brain was normalized to map onto the neonatal atlas (http://cmrm.med.jhmi.edu/) and segmented into 126 regions. Based on the trace map, regions >0.006 mm^2/s corresponding to CSF were excluded from the segmented regions (Oishi et al., 2011). A threshold of FA >0.15 was then applied (Vassar et al., 2013). Use of higher thresholds such as 0.25 FA used in adults may restrict measurements primarily to myelinated, highly ordered regions of WM. The 0.15 FA threshold was selected to balance the inclusion of less mature WM regions, which may better represent progression of development during the neonatal period, while minimizing inclusion of GM and partial volume effects. A threshold of 0.15 FA has been previously

utilized in studies of full-term and preterm infants scanned from 1 to 35 months corrected age (de Bruïne et al., 2011; Lee et al., 2012).

We examined subcortical WM defined by the JHU parcellation atlas that was well-visualized with near-term MRI and DTI, and thought to mediate motor, cognitive, or language function, illustrated in Fig. 1. We measured FA, MD, AD, and RD in projection fibers of anterior (ACR), superior (SCR), and posterior corona radiata (PCR), commissural fibers of anterior (genu) and posterior CC (splenium), projection fibers of anterior (ALIC) and posterior (PLIC) internal capsule, cerebral peduncle (CereP), retrolenticular part of the internal capsule (RLC), posterior thalamic radiation (PTR) and sagittal stratum (SS). Association fibers, including the external capsule (EC) and superior longitudinal fasciculus (SLF), as well as limbic WM structures of the fornix and stria terminalis (StriaT), were analyzed.

Relative volumes were calculated for each region to determine percent volume above the FA >0.15 threshold, relative to original volumes identified by the neonatal atlas. Regions selected with the FA >0.15 threshold were then mapped onto the FA, trace, AD, and RD images, and regional values were obtained. Mean diffusivity (MD), an average of the three directions of diffusion $(\lambda_1 + \lambda_2 + \lambda_3) / 3$ was calculated from the trace image.

Statistical analysis

To assess anterior versus posterior differences in microstructural development, FA, MD, AD, and RD values were compared between anterior, superior, and posterior regions of the CR, and between anterior and posterior regions of the CC and IC, using paired t-tests. Differences in DTI values were compared between adjacent regions in the central-to-peripheral spatial orientation, in projection fibers of the PLIC, RLC, PTR, and SS, and in association fibers of the EC and SLF, using paired t-tests. Left and right values for each region were averaged to perform the paired t-tests, with Bonferroni correction for multiple comparisons within regions.

Regional rates of microstructural development were assessed by calculating partial correlations between DTI and PMA-at-scan, controlling GA-at-birth. The influence of GA-at-birth was also examined by calculating partial correlations between DTI and GA-at-birth, controlling PMA-at-scan. Left and right values for each region were averaged to perform Partial correlations. Significance was reported with alpha 0.0125 to adjust for multiple comparisons within regions.

Consistency of evidence on regional brain development was assessed by comparison of DTI data from the current study with previously reported data in full-term neonates, using non-parametric Spearman's correlation. Statistical calculations were performed with SPSS 21.0 (SPSS, Chicago, IL).

Results

Table 1 lists demographic characteristics of all participants with MRI, DTI, and the subset population in this analysis, scanned at PMA of 34.7–38.6 weeks. Fig. 1 shows spatial orientation of regions defined by the neonatal atlas and FA >0.15 threshold.

Mean DTI values are reported for each region (Fig. 2, Table 2). Posterior aspects of the CR and IC had significantly higher FA, and lower MD and RD compared to anterior aspects. Posterior aspects of the CC (splenium) had higher FA compared to anterior aspects (genu). Genu and splenium RD values were not significantly different. In the posterior CR, AD

values were lower compared to anterior regions of the CR; however, in the posterior CC and IC, AD values were higher compared to anterior regions.

Centrally-located WM tracts demonstrated higher FA and lower RD values than tracts located more peripherally. Among projection fibers of PLIC, RLC, PTR, and SS, FA progressively decreased and RD values increased, corresponding to relative spatial orientation of these tracts from central to peripheral regions of the brain (Fig. 2 and Table 2). Centrally-located association fibers of the EC had significantly higher FA, and lower MD, AD, and RD than the SLF. Centrally-located projection fibers of the PLIC and CereP and commissural fibers of the genu and splenium demonstrated higher FA compared to peripherally-located association fibers, the EC and SLF (Fig. 2). The central-to-peripheral pattern was most evident based on FA and, to a lesser extent, evident in MD, AD and RD values. The PLIC consistently demonstrated diffusion measurements suggestive of the most advanced level of development and organization at this age based on FA, MD, AD, and RD (Table 2).

Comparison of consistency of the relative order of FA and MD values in 18 brain regions indicated strong, significant correlations between the current study and a study of full-term infants by Oishi et al. (2011) also using the JHU neonatal atlas. The Spearman's correlation based on FA was r = .889 (R^2 = 0.790); for MD it was r = .908 (R^2 = 0.824).

Fig. 3 shows the atlas-based selection of brain region volumes with application of FA >0.15 threshold within each region, reported as percentage of total regional volume. The PLIC, CereP, RLC, splenium, fornix, and StriaT had the highest percent volumes selected (>90% total volume) using the threshold of FA >0.15.

The majority of WM regions had significant correlations with PMA-at-scan, demonstrating higher FA, and lower MD, AD, and RD, with increased PMA-at-scan, when correcting for GA-at-birth (Table 3), and without correcting for GA-at-birth (Fig. 4).

Diffusion measures within the ALIC had the highest correlations with PMA-at-scan, as ALIC MD (r = –.545, p = .000) and RD (r = –.540, p = .000) decreased most with PMA-at-scan, controlling for GA-at-birth. The ALIC, RLC, and EC demonstrated significant negative correlations between RD and PMA-at-scan ($p \leq .001$) (Table 3).

A weak trend was observed between GA-at-birth and PMA-at-scan (r = –.284, p = .058), indicating that neonates with higher GA-at-birth were generally scanned slightly earlier than neonates with lower GA-at-birth. There was no relationship between GA-at-birth and FA values in any brain regions. However, MD and AD values in the EC and putamen, and AD values in the ALIC and RLC, demonstrated significant, positive correlations with GA-at-birth ($p < .0125$), controlling for PMA-at-scan (Table 4).

Discussion

Knowledge of temporal–spatial trajectories of regional brain development at near-term age is an essential first step to identifying regional microstructure that may have prognostic value at this age. In this paper we investigated brain development in VLBW preterm infants using DTI, an imaging method which has been previously found to be a sensitive tool for examining brain development (Dubois et al., 2006, 2008; Hüppi and Dubois, 2006; Lee et al., 2012; Oishi et al., 2011). We observed regional patterns of higher FA and lower RD, suggestive of more advanced microstructural development, in posterior compared to anterior regions of subcortical WM structures, and in central compared to peripheral WM regions. Relationships between diffusion measures in WM structures and PMA-at-scan were found, suggestive of region-specific rates of microstructural development. This paper is one of the

first to use semi-automated atlas-based analysis of DTI to assess regional microstructure in developing WM tracts at near-term age.

The majority of current knowledge about WM development and timing of myelination in the infant brain has been obtained from post-mortem anatomical studies (Brody et al., 1987; Huang et al., 2009; Meng et al., 2012; Yakovlev and Lecours, 1967) animal models (Bockhorst et al., 2008), and more recent, in vivo fetal DTI morphometric studies (Rajagopalan et al., 2012; Yoshida et al., 2013; Zanin et al., 2011). In preterm infants between 27 and 42 weeks GA, FA has been demonstrated to increase, and MD to decrease, with development (Aeby et al., 2009; Berman et al., 2009; Partridge et al., 2004). Our results corroborate and build on these past studies, in a larger neonatal population and reporting relative development in 19 subcortical WM regions, using an atlas-based semi-automated approach.

Histological studies of the brain at term-equivalent age have documented initial myelination primarily within the brain stem, cerebellar WM, PLIC, and some WM tracts extending into the thalamus and basal ganglia (Brody et al., 1987; van der Knaap and Valk, 1990; Yakovlev and Lecours, 1967). Although the majority of WM structures have not begun myelination, early stages of myelination cellular growth, including oligodendrocyte proliferation, may generate quantifiable change on DTI during the fetal period (Huang et al., 2006, 2009).

Rapid growth and neurogenesis occur during the third trimester of fetal brain development (Brody et al., 1987; Dobbing and Sands, 1973; Dubois et al., 2008; Huang et al., 2006; Kinney et al., 1988; Nossin-Manor et al., 2013), but may be altered as a result of preterm birth (Malik et al., 2013). Previous studies have demonstrated that, at term-equivalent age, preterm infant brain volumes differ from term-born neonates, in reduced cerebral volumes, cortical volumes (Inder et al., 2005; Thompson et al., 2006, 2013) and WM maturity (Hüppi et al., 1998; Lee et al., 2012; Rose et al., 2008). Furthermore, brain regions undergoing pre-myelination oligodendritic proliferation and formation of axonal–glial synapses may be particularly vulnerable to hypoxic ischemia and diffuse cerebral WM injury (Liu et al., 2013). Despite these differences, preterm and full-term brain developmental trajectories during the first year of life are similar in terms of a progressive decrease in water diffusion due to proliferation of oligodendrocytes and general WM maturation (Dubois et al., 2008; Lee et al., 2012; Serag et al., 2012).

Evidence of posterior-to-anterior development

During the first year of life, WM development within a given structure was observed to progress from a posterior to anterior direction in full-term infants, using myelin-specific MRI, a multicomponent relaxation analysis (Deoni et al., 2011). Our DTI data is consistent with these findings and suggests a posterior to anterior direction of WM maturation within the CR, IC, and in the CC to a lesser degree, as demonstrated by higher FA and lower MD and RD values in more posterior regions (Fig. 2, Table 2).

The SCR and PCR demonstrated higher FA and lower MD and RD values relative to the ACR. The PCR also had the highest percent volume of fibers with FA >0.15 (77% on the L, 79% on the R), compared to the ACR (27% on the L, 23% on the R) (Fig. 3) Similarly, posterior regions of the CC and IC demonstrated higher percent volumes compared to anterior regions, likely reflecting earlier maturation in posterior regions.

The splenium has been found to myelinate earlier and more rapidly than the genu during the first year of life. Splenium myelination was estimated to start at 3 months of age and progress to the genu by 7–9 months of age (Provenzale et al., 2012). Our data, collected at

35–39 week PMA are consistent with previous findings of higher FA and AD within the splenium compared to the genu in preterm infants scanned at 40–62 weeks and in healthy full-term infants scanned during the first months of life (de Bruïne et al., 2011; Gilmore et al., 2007). RD was similar within the genu and splenium, which may be expected as RD is thought to reflect myelination, which has likely not yet begun in the CC.

The ALIC and PLIC demonstrated a high degree of differential development. Histological studies found visible myelination in the PLIC at 36–38 weeks (Brody et al., 1987; Cowan and de Vries, 2005), estimated to begin at 32 week PMA and reach full myelination by 46 week PMA (Cowan and de Vries, 2005). In contrast, the ALIC did not show evidence of myelination until around 46 week PMA and did not appear fully myelinated until 4–5 month post-term (Cowan and de Vries, 2005). The current study found higher FA, and lower MD and RD, in the PLIC compared to the ALIC, consistent with a posterior-to-anterior progression of maturation within the IC.

The FA values of subcortical nuclei WM were relatively low (Fig. 2). The more anterior located caudate head demonstrated substantially higher MD, AD, and RD values and has been found to myelinate around 35–36 weeks compared to the more posterior located thalamus, which is known to myelinate earlier around 24–25 weeks and noted to be more vulnerable to injury in the preterm population (Huang and Castillo, 2008).

Evidence of central-to-peripheral development

DTI measures suggestive of earlier microstructural development were observed in more inferior and central projection fibers (CereP and PLIC), compared to peripherally-located projection fibers (CR) and association fibers (SLF and EC). Among projection fibers, progressively higher FA was observed in central compared to peripheral regions of the PLIC, RLC, PTR, and SS (Figs. 2 and 5). Furthermore, among association fibers, the more centrally-located EC had higher FA, and lower MD, AD, and RD compared to the SLF (Fig. 2, Table 2). The SLF has been reported to be one of the slowest developing WM tracts (Paus et al., 1999; Thompson et al., 2000) and at term-equivalent age, has not yet started to myelinate (Huang et al., 2006; Kinney et al., 1988; Oishi et al., 2011). Based on relative FA, MD, and RD values, our findings suggest that the PLIC, RLC, and CereP have the earliest microstructural development at near-term age, and that the least mature structures are the ACR and SLF. These findings may relate to the central location of the germinal matrix (Liu et al., 2013). The temporal–spatial pattern is consistent with debated theory that “ontogeny recapitulates phylogeny”. In the case of brain development, this pattern appears to occur, given the earlier development of inferior and centrally-located primitive evolutionary structures, such as the brain stem, mid-brain, and lower CST, followed by development of more advanced, peripherally-located brain structures.

Other possible explanations for this observed trend include the lower signal-to-noise ratio generally observed in more cortical regions, or the difficulty in accurately segmenting and analyzing small WM regions with low FA, where partial volume effects likely occur. Crossing fibers may also contribute to variation in diffusion measurements in regions such as the CR, a region known to have a substantial number of crossing fibers in the adult brain (Dubois et al., 2008; Oishi et al., 2011). Thus, FA measures must be interpreted based on both microscopic (e.g., axonal development and myelination) as well as macroscopic factors (e.g., crossing fibers) (Oishi et al., 2011). The high MD and RD values of the ACR, compared to values in the SCR and PCR, however, suggests a lower degree of maturation of ACR in relation to more posterior regions of the CR.

Regional volumes

Segmentation of WM within the neonatal brain commonly involves application of FA thresholds (Vassar et al., 2013). Fig. 3 shows the PLIC, Cere P, and RLC had the highest percent volumes with FA >0.15, consistent with previous anatomical studies that found myelination of the CST during the third trimester. Limbic fibers (fornix and StriaT), the CC, and projection fibers of the PTR and SS also had volumes in which >80% was above the FA >0.15 threshold. These findings indicate that these tracts have high degree of anisotropic diffusion, suggestive of organization and increased density of developing WM fibers. These tracts are all known to be dense WM fibers in the adult brain, and the relatively high anisotropy is consistent with previous anatomical findings in adults.

Regions with lowest percent volume were the ACR and SLF, regions of future WM tracts that are likely undeveloped at near-term age. Analysis of WM within subcortical nuclei also demonstrated low percent volume. These regions contain both WM and GM, and likely the FA >0.15 threshold eliminated most GM and included only WM thalamocortical and other projection fibers developing during this near-term period (Counsell et al., 2002; van der Knaap and Valk, 1990). Interpretation of DTI in regions with relatively low percent volumes must be done cautiously (Vassar et al., 2013). Conversely, identification of regions with relatively high degree of anisotropy at near-term age may be helpful in determining tracts that are relatively well-developed, more likely to be accurately selected with a semi-automated atlas, and thus may hold prognostic value for future function.

Consistent regional patterns of WM development

Consistency was assessed between regional patterns of development found in our population of near-term infants and data from a study of 22 full-term infants scanned at 37–53 week PMA by Oishi et al. (2011), analyzed with DiffeoMap neonatal atlas (Table 5). As expected, in our near-term population, FA values were lower and MD values were higher compared to the full-term population, however, the relative order of regions from highest-to-lowest FA and lowest-to-highest MD showed a very high degree of agreement between studies (Oishi et al., 2011), suggesting consistent evidence on the pattern of regional WM development.

Region specific rates of development

Regional rates of development were estimated by investigating the influence of PMA-at-scan, controlling for GA-at-birth (Table 3, Fig. 5). Our cross-sectional observations from near-term infants 35–39 week PMA are consistent with findings of several studies that examined DTI from birth to 2 years and found a progressive increase in FA and decrease in AD and MD with age in WM pathways (Gao et al., 2008; Geng et al., 2012; Yoshida et al., 2013). Increasing FA at near-term age may indicate regions with increasing WM fiber diameter, density, tract coherence, or myelination (Basser, 1995; Basser and Pierpaoli, 1996). Decreasing MD during this period can likely be attributed to an overall decrease in brain water content, and also to proliferation of cells, intercellular compartments, and membranes during myelination stages of tract development (Dubois et al., 2008; Hüppi et al., 1998). Myelination was found to be best represented by RD (Song et al., 2002) as diffusion perpendicular to the axons becomes more restricted by myelin.

Regions that demonstrated the strongest correlations with PMA-at-scan were the ALIC, RLC, EC, ACR, and PLIC. At near-term age, these regions are likely undergoing rapid development, quantifiable by changes in diffusion. Changes in diffusion may be primarily driven by decreases in water concentration in the neonatal brain, and may also be influenced by microstructure development during stages of myelination. During early myelination stages of fiber development or myelination gliosis (Zanin et al., 2011) there is proliferation in precursor oligodendrocytes and a decrease in water content that occurs isotropically

(Aeby et al., 2009; Dubois et al., 2008; Gilmore et al., 2007; Liu et al., 2013). Further fiber development and myelination involve ensheathment of axons by oligodendrocytes and decreased cell membrane permeability and cell spacing.

Whether an initial high rate of change in diffusion or a specific profile of diffusion values may signify the onset of myelination, warrants further study. Dubois et al. (2008) and Zanin et al. (2011), who examined in vivo fetal brain development on DTI, found that the CC demonstrated no change in FA, with decreases in MD, RD, and AD, with PMA. This profile of DTI values has been interpreted to indicate developing WM that has not started to myelinate. Early myelination processes, or myelination gliosis (Zanin et al., 2011), involve proliferation of precursor oligodendrocytes associated with isotropic production of glial matter in the extracellular space and initial axonal ensheathment by pioneer processes (Back et al., 2002). This is followed by regression of cytoplasmic arborization and progressive ensheathment of axons, compaction of myelin sheaths, and incorporation of myelin binding protein (Back et al., 2002). Interpretation of DTI profiles that may correspond to specific phases of WM microstructural development has been proposed and has considered relative values and rate of change of DTI measures (Dubois et al., 2008; Zanin et al., 2011). Identification of different stages of WM development based on DTI will provide valuable clinical insight into brain development and selective vulnerability to WM injury.

We found that DTI values in the CC demonstrated no significant correlation with PMA-at-scan at near-term age. While the basic structure of the CC is visible at approximately 18–20 week GA (Malinger and Zakut, 1993), myelination is estimated to start at 3 months of age and progress to the genu by 7–9 months of age (Provenzale et al., 2012). Growth and myelination of the CC continue for at least the first two years of post-natal life (Keshavan et al., 2002). Provenzale et al. (2012) found substantial increases in FA, and decreases in MD, AD, and RD in the CC during the 3–9 month postnatal period. The lack of correlations between PMA-at-scan and CC DTI values in our cohort likely reflects the later onset of myelination. It could also suggest that CC growth and development are highly variable, as observed in Partridge et al. (2004). However, variability of CC DTI values at near-term age within our cohort was relatively low and comparable to other regions (Table 2, Fig. 4). Dubois et al. (2008) also found no significant change in FA measured in the CC among a cohort of healthy, term-born infants at approximately 50 week PMA, but found a significant decrease in MD with PMA attributed to particularly tight bundling of fibers within the CC that may mask changes in anisotropy. Though the CC demonstrates relatively high FA (Fig. 2), suggestive of dense and organized structure, microstructural changes may be subtle during this near-term period, before the onset of CC myelination. Further analysis with longitudinal imaging would allow for more detailed understanding of CC development, a region that may correlate with later neurodevelopmental function (Counsell et al., 2008; van Kooij et al., 2012).

Oishi et al. (2011) suggested that in infants, fibers located further from the brainstem (such as the CR, PTR, and SS) have MD values that decrease more rapidly than tracts such as the PLIC, RLC, and CereP located closer to the brainstem. In our study, ALIC MD and RD values demonstrated the most significant, negative correlation with PMA-at-scan. PLIC, RLC, EC, ACR and thalamus MD and RD were also negatively correlated with PMA-at-scan ($p \leq .0125$). These correlations are consistent with findings in full-term infants (Oishi et al., 2011) and previous anatomical studies that suggest that at near-term age, myelination is occurring in inferior portions of the CST, compared to more superior regions of the CR, CC and SLF which may not begin myelination for several months.

Influence of GA-at-birth

The effect of GA on near-term DTI measures of WM was assessed, given the association between degree of prematurity and reduced WM volume, WM immaturity, and adverse neurodevelopmental outcomes (Aarnoudse-Moens et al., 2009; Anderson and Doyle, 2003; Constantinou et al., 2005). Most regions did not exhibit a significant relation between GA and DTI values, when controlling for PMA-at-scan (Table 4). No relation between GA and FA was found in any region. Few studies have investigated the role of prematurity on WM maturation, independent of other variables, and isolating the role of GA is diffi-cult due to multiple co-morbidities that may influence brain maturation. However, Bonifacio et al. (2010) and Shim et al. (2012) found that WM maturity is generally independent of GA after controlling for other clinical variables. We observed in the EC and putamen significant positive correlations between GA and MD and AD that suggest relatively slower development of these regions in infants with higher GA. If this finding is corroborated, one possible explanation may be accelerated growth after birth in these regions. Another explanation may be that certain treatments are administered more aggressively to neonates with lower GA and may have protective influence on development.

Microstructural development and selective vulnerability at near-term age

Myelination may be selectively vulnerable to injury (Hüppi et al., 1998; Liu et al., 2013; Miller and Ferriero, 2009; Neil et al., 2002; Volpe, 2003). Periventricular WM has been found to be particularly vulnerable to injury at the end of the second trimester, associated with spastic CP (Johnston and Hoon, 2000). In contrast, injury to subcortical nuclei identified at term-age may be associated with quadriplegic and dyskinetic CP, suggesting that different regions may be more vulnerable at different developmental time points (Johnston and Hoon, 2000; Miller and Ferriero, 2009). The influence of severity of injury, development of vascularization, and stage of WM myelination on selective vulnerability requires further investigation.

Early stages of myelination involve proliferation of precursor oligodendrocytes, which may be particularly vulnerable to injury. The dynamic role of oligodendrocytes in modulation of axonal transmission and activity-dependent growth involves more complex physiology than previously recognized (Fields, 2008). In addition to proliferation of precursor oligodendrocytes, myelination involves development of ion channels, neurotransmitter receptors, and signaling processes and requires high metabolic activity that may be particularly vulnerable to hypoxic events. These myelination processes may also generate rapid rates of change in diffusion. Further research is needed to investigate if rate of change or profile of DTI measures may provide biomarkers of selectively vulnerable WM at near-term age.

Conclusion

This research reports on semi-automated atlas-based analysis of DTI that examines regional microstructure in developing WM tracts at near-term age. We observed regional patterns of higher FA and lower RD, suggestive of more advanced microstructural development, in posterior compared to anterior WM regions and in central compared to peripheral WM regions. Evidence of region-specific rates of microstructural development in relation to PMA-at-scan was observed. Most regions did not exhibit a significant correlation between DTI values, and GA-at-birth with the exception of the EC and putamen, suggesting differential effects of GA on regional development. Developmental patterns observed in this preterm population are similar to those previously reported in full-term infants, indicating a consistent pattern of regional WM development. Quantifying regional patterns of brain microstructure development in the preterm population at near-term age may clarify brain

developmental trajectories and selective vulnerability to injury. Limitations of this study include the cross-sectional design. Sequential neuroimaging during the near-term period would reveal individual temporal–spatial trajectories of development. Interpretation of relative regional DTI values must be done cautiously, as these may reflect both microstructural architecture and/or development, and may be influenced by imaging parameters. Future studies may determine whether regional patterns of microstructural development could provide early prognostic bio-markers that may ultimately guide early intervention aimed at reducing neurodevelopmental disabilities.

Acknowledgments

We wish to thank Alex Sox-Harris for valuable statistical consultation. This research is supported in part by the NIH Clinical and Translational Science Award 1UL1 RR025744 for the Stanford Center for Clinical and Translational Education and Research (Spectrum) and by the Lucile Packard Foundation for Children's Health. This material is based upon work supported by the National Science Foundation Graduate Research Fellowship under Grant No. DGE-1147470.

Abbreviations

VLBW	very-low-birth-weight
GA	gestational age
PMA	postmenstrual age
FA	fractional anisotropy
MD	mean diffusivity
AD	axial diffusivity
RD	radial diffusivity
CR	corona radiata
ACR	anterior corona radiata
SCR	superior corona radiata
PCR	posterior corona radiata
CC	corpus callosum
IC	internal capsule
ALIC	anterior limb of the internal capsule
PLIC	posterior limb of the internal capsule
CereP	cerebral Peduncle
RLC	retrolenticular part of internal capsule
PTR	posterior thalamic radiation
SS	sagittal stratum
EC	external capsule
SLF	superior longitudinal fasciculus
StriaT	stria terminalis

References

Aarnoudse-Moens CSH, Weisglas-Kuperus N, van Goudoever JB, Oosterlaan J. Meta-analysis of neurobehavioral outcomes in very preterm and/or very low birth weight children. Pediatrics. 2009; 124(2):717–728. http://dx.doi.org/10.1542/peds.2008-2816. [PubMed: 19651588]

Aeby A, Liu Y, De Tiège X, Denolin V, David P, Balériaux D, Van Bogaert P. Maturation of thalamic radiations between 34 and 41 weeks' gestation: a combined voxel-based study and probabilistic tractography with diffusion tensor imaging. AJNR Am. J. Neuroradiol. 2009; 30(9):1780–1786. http://dx.doi.org/10.3174/ajnr.A1660. [PubMed: 19574497]

Aeby, Alec; De Tiège, X.; Creuzil, M.; David, P.; Balériaux, D.; Van Overmeire, B.; Van Bogaert, P. Language development at 2 years is correlated to brain microstructure in the left superior temporal gyrus at term equivalent age: a diffusion tensor imaging study.. NeuroImage. 2013. http://dx.doi.org/10.1016/j.neuroimage.2013.03.076

Anderson P, Doyle LW. Neurobehavioral outcomes of school-age children born extremely low birth weight or very preterm in the 1990s. JAMA. 2003; 289(24):3264–3272. http://dx.doi.org/10.1001/jama.289.24.3264. [PubMed: 12824207]

Arzoumanian Y, Mirmiran M, Barnes PD, Woolley K, Ariagno RL, Moseley ME, Atlas SW. Diffusion tensor brain imaging findings at term-equivalent age may predict neurologic abnormalities in low birth weight preterm infants. AJNR Am. J. Neuroradiol. 2003; 24(8):1646–1653. [PubMed: 13679287]

Back SA, Luo NL, Borenstein NS, Volpe JJ, Kinney HC. Arrested oligodendrocyte lineage progression during human cerebral white matter development: dissociation between the timing of progenitor differentiation and myelinogenesis. J. Neuropathol. Exp. Neurol. 2002; 61(2):197–211. [PubMed: 11853021]

Basser PJ. Inferring microstructural features and the physiological state of tissues from diffusion-weighted images. NMR Biomed. 1995; 8(7–8):333–344. [PubMed: 8739270]

Basser PJ, Pierpaoli C. Microstructural and physiological features of tissues elucidated by quantitative-diffusion-tensor MRI. J. Magn. Reson. Ser. B. 1996; 111(3):209–219. [PubMed: 8661285]

Benini, R.; Dagenais, L.; Shevell, MI. Normal imaging in patients with cerebral palsy: what does it tell us?. J. Pediatr. 2012. http://dx.doi.org/10.1016/j.jpeds.2012.07.044

Berman JI, Glass HC, Miller SP, Mukherjee P, Ferriero DM, Barkovich AJ, Henry RG. Quantitative fiber tracking analysis of the optic radiation correlated with visual performance in premature newborns. AJNR Am. J. Neuroradiol. 2009; 30(1):120–124. http://dx.doi.org/10.3174/ajnr.A1304. [PubMed: 18832665]

Bockhorst KH, Narayana PA, Liu R, Ahobila-Vijjula P, Ramu J, Kamel M, Perez-Polo JR. Early postnatal development of rat brain: in vivo diffusion tensor imaging. J. Neurosci. Res. 2008; 86(7): 1520–1528. http://dx.doi.org/10.1002/jnr.21607. [PubMed: 18189320]

Bonifacio SL, Glass HC, Chau V, Berman JI, Xu D, Brant R, Ferriero DM. Extreme premature birth is not associated with impaired development of brain microstructure. J. Pediatr. 2010; 157(5):726–732. e1. http://dx.doi.org/10.1016/j.jpeds.2010.05.026. [PubMed: 20598316]

Brody BA, Kinney HC, Kloman AS, Gilles FH. Sequence of central nervous system myelination in human infancy. I. An autopsy study of myelination. J. Neuropathol. Exp. Neurol. 1987; 46(3):283–301. [PubMed: 3559630]

Chen Y, An H, Zhu H, Jewells V, Armao D, Shen D, Lin W. Longitudinal regression analysis of spatial–temporal growth patterns of geometrical diffusion measures in early postnatal brain development with diffusion tensor imaging. NeuroImage. 2011; 58(4):993–1005. http://dx.doi.org/10.1016/j.neuroimage.2011.07.006. [PubMed: 21784163]

Constantinou JC, Adamson-Macedo EN, Mirmiran M, Ariagno RL, Fleisher BE. Neurobehavioral assessment predicts differential outcome between VLBW and ELBW preterm infants. J. Perinatol. 2005; 25(12):788–793. http://dx.doi.org/10.1038/sj.jp.7211403. [PubMed: 16292337]

Counsell SJ, Maalouf EF, Fletcher AM, Duggan P, Battin M, Lewis HJ, Rutherford MA. MR imaging assessment of myelination in the very preterm brain. AJNR Am. J. Neuroradiol. 2002; 23(5):872–881. [PubMed: 12006296]

Counsell SJ, Edwards AD, Chew ATM, Anjari M, Dyet LE, Srinivasan L, Cowan FM. Specific relations between neurodevelopmental abilities and white matter microstructure in children born preterm. Brain. 2008; 131(Pt 12):3201–3208. http://dx.doi.org/10.1093/brain/awn268. [PubMed: 18952670]

Cowan FM, de Vries LS. The internal capsule in neonatal imaging. Semin. Fetal Neonatal Med. 2005; 10(5):461–474. http://dx.doi.org/10.1016/j.siny.2005.05.007. [PubMed: 16002354]

De Bruïne FT, van Wezel-Meijler G, Leijser LM, van den Berg-Huysmans AA, van Steenis A, van Buchem MA, van der Grond J. Tractography of developing white matter of the internal capsule and corpus callosum in very preterm infants. Eur. Radiol. 2011; 21(3):538–547. http://dx.doi.org/10.1007/s00330-010-1945-x. [PubMed: 20835871]

Deoni SCL, Mercure E, Blasi A, Gasston D, Thomson A, Johnson M, Murphy DGM. Mapping infant brain myelination with magnetic resonance imaging. J. Neurosci. Off. J. Soc. Neurosci. 2011; 31(2):784–791. http://dx.doi.org/10.1523/JNEUROSCI.2106-10.2011.

Dobbing J, Sands J. Quantitative growth and development of human brain. Arch. Dis. Child. 1973; 48(10):757–767. http://dx.doi.org/10.1136/adc.48.10.757. [PubMed: 4796010]

Dubois J, Hertz-Pannier L, Dehaene-Lambertz G, Cointepas Y, Le Bihan D. Assessment of the early organization and maturation of infants' cerebral white matter fiber bundles: a feasibility study using quantitative diffusion tensor imaging and tractography. NeuroImage. 2006; 30(4):1121–1132. http://dx.doi.org/10.1016/j.neuroimage.2005.11.022. [PubMed: 16413790]

Dubois, Jessica; Dehaene-Lambertz, G.; Perrin, M.; Mangin, J-F.; Cointepas, Y.; Duchesnay, E.; Hertz-Pannier, L. Asynchrony of the early maturation of white matter bundles in healthy infants: quantitative landmarks revealed noninvasively by diffusion tensor imaging. Hum. Brain Mapp. 2008; 29(1):14–27. http://dx.doi.org/10.1002/hbm.20363. [PubMed: 17318834]

Fields RD. Oligodendrocytes changing the rules: action potentials in glia and oligodendrocytes controlling action potentials. Neuroscientist. 2008; 14(6):540–543. http://dx.doi.org/10.1177/1073858408320294. [PubMed: 19029057]

Gao W, Lin W, Chen Y, Gerig G, Smith JK, Jewells V, Gilmore JH. Temporal and spatial development of axonal maturation and myelination of white matter in the developing brain. Am. J. Neuroradiol. 2008; 30(2):290–296. http://dx.doi.org/10.3174/ajnr.A1363. [PubMed: 19001533]

Geng X, Gouttard S, Sharma A, Gu H, Styner M, Lin W, Gilmore JH. Quantitative tract-based white matter development from birth to age 2 years. NeuroImage. 2012; 61(3):542–557. http://dx.doi.org/10.1016/j.neuroimage.2012.03.057. [PubMed: 22510254]

Gilmore JH, Lin W, Corouge I, Vetsa YSK, Smith JK, Kang C, Gerig G. Early postnatal development of corpus callosum and corticospinal white matter assessed with quantitative tractography. AJNR Am. J. Neuroradiol. 2007; 28(9):1789–1795. http://dx.doi.org/10.3174/ajnr.A0651. [PubMed: 17923457]

Huang BY, Castillo M. Hypoxic–ischemic brain injury: imaging findings from birth to adulthood. Radiographics. 2008; 28(2):417–439. http://dx.doi.org/10.1148/rg.282075066. [PubMed: 18349449]

Huang, Hao; Zhang, J.; Wakana, S.; Zhang, W.; Ren, T.; Richards, LJ.; Mori, S. White and gray matter development in human fetal, newborn and pediatric brains. NeuroImage. 2006; 33(1):27–38. http://dx.doi.org/10.1016/j.neuroimage.2006.06.009. [PubMed: 16905335]

Huang H, Xue R, Zhang J, Ren T, Richards LJ, Yarowsky P, Mori S. Anatomical characterization of human fetal brain development with diffusion tensor magnetic resonance imaging. J. Neurosci. 2009; 29(13):4263–4273. http://dx.doi.org/10.1523/JNEUROSCI.2769-08.2009. [PubMed: 19339620]

Hüppi, Petra S.; Dubois, J. Diffusion tensor imaging of brain development. Semin. Fetal Neonatal Med. 2006; 11(6):489–497. http://dx.doi.org/10.1016/j.siny.2006.07.006. [PubMed: 16962837]

Hüppi PS, Maier SE, Peled S, Zientara GP, Barnes PD, Jolesz FA, Volpe JJ. Microstructural development of human newborn cerebral white matter assessed in vivo by diffusion tensor magnetic resonance imaging. Pediatr. Res. 1998; 44(4):584–590. http://dx.doi.org/10.1203/00006450-199810000-00019. [PubMed: 9773850]

Inder TE, Warfield SK, Wang H, Hüppi PS, Volpe JJ. Abnormal cerebral structure is present at term in premature infants. Pediatrics. 2005; 115(2):286–294. http://dx.doi.org/10.1542/peds.2004-0326. [PubMed: 15687434]

Johnston MV, Hoon AH. Possible mechanisms in infants for selective basal ganglia damage from asphyxia, kernicterus, or mitochondrial encephalopathies. J. Child Neurol. 2000; 15(9):588–591. http://dx.doi.org/10.1177/088307380001500904. [PubMed: 11019789]

Keshavan MS, Diwadkar VA, DeBellis M, Dick E, Kotwal R, Rosenberg DR, Pettegrew JW. Development of the corpus callosum in childhood, adolescence and early adulthood. Life Sci. 2002; 70(16):1909–1922. [PubMed: 12005176]

Kidokoro H, Anderson PJ, Doyle LW, Neil JJ, Inder TE. High signal intensity on T2-weighted MR imaging at term-equivalent age in preterm infants does not predict 2-year neurodevelopmental outcomes. AJNR Am. J. Neuroradiol. 2011; 32(11):2005–2010. http://dx.doi.org/10.3174/ajnr.A2703. [PubMed: 21960493]

Kinney HC, Brody BA, Kloman AS, Gilles FH. Sequence of central nervous system myelination in human infancy. II. Patterns of myelination in autopsied infants. J. Neuropathol. Exp. Neurol. 1988; 47(3):217–234. [PubMed: 3367155]

Kinney HC, Karthigasan J, Borenshteyn NI, Flax JD, Kirschner DA. Myelination in the developing human brain: biochemical correlates. Neurochem. Res. 1994; 19(8):983–996. [PubMed: 7800125]

Lee, AY.; Jang, SH.; Lee, E.; Ahn, SH.; Cho, HK.; Jo, HM.; Son, SM. Radiologic differences in white matter maturation between preterm and full-term infants: TBSS study.. Pediatr. Radiol. 2012. http://dx.doi.org/10.1007/s00247-012-2545-5

Liu, X-B.; Shen, Y.; Plane, JM.; Deng, W. Vulnerability of premyelinating oligodendrocytes to white matter damage in neonatal brain injury.. Neurosci. Bull. 2013. http://dx.doi.org/10.1007/s12264-013-1311-5

Löbel U, Sedlacik J, Güllmar D, Kaiser WA, Reichenbach JR, Mentzel H-J. Diffusion tensor imaging: the normal evolution of ADC, RA, FA, and eigenvalues studied in multiple anatomical regions of the brain. Neuroradiology. 2009; 51(4):253–263. http://dx.doi.org/10.1007/s00234-008-0488-1. [PubMed: 19132355]

Malik S, Vinukonda G, Vose LR, Diamond D, Bhimavarapu BBR, Hu F, Ballabh P. Neurogenesis continues in the third trimester of pregnancy and is suppressed by premature birth. J. Neurosci. Off. J. Soc. Neurosci. 2013; 33(2):411–423. http://dx.doi.org/10.1523/JNEUROSCI.4445-12.2013.

Malinger G, Zakut H. The corpus callosum: normal fetal development as shown by transvaginal sonography. AJ. Am. J. Roentgenol. 1993; 161(5):1041–1043. http://dx.doi.org/10.2214/ajr.161.5.8273605.

Meng H, Zhang Z, Geng H, Lin X, Feng L, Teng G, Liu S. Development of the subcortical brain structures in the second trimester: assessment with 7.0-T MRI. Neuroradiology. 2012; 54(10):1153–1159. http://dx.doi.org/10.1007/s00234-012-1069-x. [PubMed: 22811291]

Miller SP, Ferriero DM. From selective vulnerability to connectivity: insights from newborn brain imaging. Trends Neurosci. 2009; 32(9):496–505. http://dx.doi.org/10.1016/j.tins.2009.05.010. [PubMed: 19712981]

Mukherjee P, Miller JH, Shimony JS, Philip JV, Nehra D, Snyder AZ, McKinstry RC. Diffusion-tensor MR imaging of gray and white matter development during normal human brain maturation. AJNR Am. J. Neuroradiol. 2002; 23(9):1445–1456. [PubMed: 12372731]

Neil J, Miller J, Mukherjee P, Hüppi PS. Diffusion tensor imaging of normal and injured developing human brain — a technical review. NMR Biomed. 2002; 15(7–8):543–552. http://dx.doi.org/10.1002/nbm.784. [PubMed: 12489100]

Nossin-Manor R, Card D, Morris D, Noormohamed S, Shroff MM, Whyte HE, Sled JG. Quantitative MRI in the very preterm brain: assessing tissue organization and myelination using magnetization transfer, diffusion tensor and T1 imaging. NeuroImage. 2013; 64:505–516. http://dx.doi.org/10.1016/j.neuroimage.2012.08.086. [PubMed: 22982360]

Oishi K, Mori S, Donohue PK, Ernst T, Anderson L, Buchthal S, Chang L. Multi-contrast human neonatal brain atlas: application to normal neonate development analysis. NeuroImage. 2011; 56(1):8–20. http://dx.doi.org/10.1016/j.neuroimage.2011.01.051. [PubMed: 21276861]

Oishi K, Faria AV, Yoshida S, Chang L, Mori S. Quantitative evaluation of brain development using anatomical MRI and diffusion tensor imaging. Int. J. Dev. Neurosci. 2013; 31(7):512–524. http://dx.doi.org/10.1016/j.ijdevneu.2013.06.004. [PubMed: 23796902]

Partridge SC, Mukherjee P, Henry RG, Miller SP, Berman JI, Jin H, Vigneron DB. Diffusion tensor imaging: serial quantitation of white matter tract maturity in premature newborns. NeuroImage. 2004; 22(3):1302–1314. http://dx.doi.org/10.1016/j.neuroimage.2004.02.038. [PubMed: 15219602]

Paus T, Zijdenbos A, Worsley K, Collins DL, Blumenthal J, Giedd JN, Evans AC. Structural maturation of neural pathways in children and adolescents: in vivo study. Science (New York, N.Y.). 1999; 283(5409):1908–1911.

Pierpaoli C, Jezzard P, Basser PJ, Barnett A, Di Chiro G. Diffusion tensor MR imaging of the human brain. Radiology. 1996; 201(3):637–648. [PubMed: 8939209]

Provenzale JM, Isaacson J, Chen S. Progression of corpus callosum diffusion-tensor imaging values during a period of signal changes consistent with myelination. Am. J. Roentgenol. 2012; 198(6): 1403–1408. http://dx.doi.org/10.2214/AJR.11.7849. [PubMed: 22623555]

Rajagopalan V, Scott J, Habas PA, Kim K, Rousseau F, Glenn OA, Studholme C. Mapping directionality specific volume changes using tensor based morphometry: an application to the study of gyrogenesis and lateralization of the human fetal brain. NeuroImage. 2012; 63(2):947–958. http://dx.doi.org/10.1016/j.neuroimage.2012.03.092. [PubMed: 22503938]

Rakic P. Specification of cerebral cortical areas. Science. 1988; 241(4862):170–176. http://dx.doi.org/10.1126/science.3291116. [PubMed: 3291116]

Rose J, Mirmiran M, Butler EE, Lin CY, Barnes PD, Kermoian R, Stevenson DK. Neonatal microstructural development of the internal capsule on diffusion tensor imaging correlates with severity of gait and motor deficits. Dev. Med. Child Neurol. 2007; 49(10):745–750. http://dx.doi.org/10.1111/j.1469-8749.2007.00745.x. [PubMed: 17880643]

Rose J, Butler EE, Lamont LE, Barnes PD, Atlas SW, Stevenson DK. Neonatal brain structure on MRI and diffusion tensor imaging, sex, and neurodevelopment in very-low-birthweight preterm children. Dev. Med. Child Neurol. 2009; 51(7):526–535. http://dx.doi.org/10.1111/j.1469-8749.2008.03231.x. [PubMed: 19459915]

Rose SE, Hatzigeorgiou X, Strudwick MW, Durbridge G, Davies PSW, Colditz PB. Altered white matter diffusion anisotropy in normal and preterm infants at term-equivalent age. Magn. Reson. Med. 2008; 60(4):761–767. http://dx.doi.org/10.1002/mrm.21689. [PubMed: 18816850]

Serag A, Aljabar P, Ball G, Counsell SJ, Boardman JP, Rutherford MA, Rueckert D. Construction of a consistent high-definition spatio-temporal atlas of the developing brain using adaptive kernel regression. NeuroImage. 2012; 59(3):2255–2265. http://dx.doi.org/10.1016/j.neuroimage.2011.09.062. [PubMed: 21985910]

Shim S-Y, Jeong H-J, Son DW, Jeong JS, Oh SH, Park S-Y, Cho Z-H. Altered microstructure of white matter except the corpus callosum is independent of prematurity. Neonatology. 2012; 102(4):309–315. http://dx.doi.org/10.1159/000341867. [PubMed: 22986463]

Song S-K, Sun S-W, Ramsbottom MJ, Chang C, Russell J, Cross AH. Dysmyelination revealed through MRI as increased radial (but unchanged axial) diffusion of water. NeuroImage. 2002; 17(3):1429–1436. [PubMed: 12414282]

Spittle AJ, Cheong J, Doyle LW, Roberts G, Lee KJ, Lim J, Anderson PJ. Neonatal white matter abnormality predicts childhood motor impairment in very preterm children. Dev. Med. Child Neurol. 2011; 53:1000–1006. http://dx.doi.org/10.1111/j.1469-8749.2011.04095.x. [PubMed: 22014319]

Thompson PM, Giedd JN, Woods RP, MacDonald D, Evans AC, Toga AW. Growth patterns in the developing brain detected by using continuum mechanical tensor maps. Nature. 2000; 404(6774): 190–193. http://dx.doi.org/10.1038/35004593. [PubMed: 10724172]

Thompson DK, Warfield SK, Carlin JB, Pavlovic M, Wang HX, Bear M, Inder TE. Perinatal risk factors altering regional brain structure in the preterm infant. Brain. 2006; 130(3):667–677. http://dx.doi.org/10.1093/brain/awl277. [PubMed: 17008333]

Thompson, Deanne K.; Inder, TE.; Faggian, N.; Warfield, SK.; Anderson, PJ.; Doyle, LW.; Egan, GF. Corpus callosum alterations in very preterm infants: perinatal correlates and 2 year

neurodevelopmental outcomes. NeuroImage. 2012; 59(4):3571–3581. http://dx.doi.org/10.1016/j.neuroimage.2011.11.057. [PubMed: 22154956]

Thompson, Deanne K.; Adamson, C.; Roberts, G.; Faggian, N.; Wood, SJ.; Warfield, SK.; Inder, TE. Hippocampal shape variations at term equivalent age in very preterm infants compared with term controls: perinatal predictors and functional significance at age 7. NeuroImage. 2013; 70:278–287. http://dx.doi.org/10.1016/j.neuroimage.2012.12.053. [PubMed: 23296179]

Van der Knaap MS, Valk J. MR imaging of the various stages of normal myelination during the first year of life. Neuroradiology. 1990; 31(6):459–470. [PubMed: 2352626]

Van Kooij, Britt J.M.; van Pul, C.; Benders, MJNL.; van Haastert, IC.; de Vries, LS.; Groenendaal, F. Fiber tracking at term displays gender differences regarding cognitive and motor outcome at 2 years of age in preterm infants. Pediatr. Res. 2011; 70(6):626–632. http://dx.doi.org/10.1203/PDR.0b013e318232a963. [PubMed: 21857376]

Van Kooij BJM, de Vries LS, Ball G, van Haastert IC, Benders MJNL, Groenendaal F, Counsell SJ. Neonatal tract-based spatial statistics findings and outcome in preterm infants. AJNR Am. J. Neuroradiol. 2012; 33(1):188–194. http://dx.doi.org/10.3174/ajnr.A2723. [PubMed: 21998101]

Vassar, R.; Barnea-Goraly, N.; Rose, J. Identification of early white matter tracts in the neonatal brain: atlas-based segmentation parameters influence DTI measurements.. Presented at the 10th Annual World Congress of SBMT. Society of Brain Mapping and Therapeutics; Baltimore, MD. 2013.

Vasung L, Huang H, Jovanov-Milošević N, Pletikos M, Mori S, Kostović I. Development of axonal pathways in the human fetal fronto-limbic brain: histochemical characterization and diffusion tensor imaging. J. Anat. 2010; 217(4):400–417. http://dx.doi.org/10.1111/j.1469-7580.2010.01260.x. [PubMed: 20609031]

Volpe JJ. Cerebral white matter injury of the premature infant—more common than you think. Pediatrics. 2003; 112(1 Pt 1):176–180. [PubMed: 12837883]

Williams J, Lee KJ, Anderson PJ. Prevalence of motor-skill impairment inpreterm children who do not develop cerebral palsy: a systematic review. Dev. Med. Child Neurol. 2010; 52(3):232–237. http://dx.doi.org/10.1111/j.1469-8749.2009.03544.x. [PubMed: 20002114]

Woodward LJ, Clark CAC, Bora S, Inder TE. Neonatal white matter abnormalities an important predictor of neurocognitive outcome for very preterm children. PLoS ONE. 2012; 7(12):e51879. http://dx.doi.org/10.1371/journal.pone.0051879. [PubMed: 23284800]

Yakovlev, PI.; Lecours, A. The myelogenetic cycles of regional maturation of the brain.. In: Minkowski, A., editor. Regional Development of the Brain in Early Life. Blackwell; Oxford: 1967. p. 3-70.

Yoshida S, Oishi K, Faria AV, Mori S. Diffusion tensor imaging of normal brain development. Pediatr. Radiol. 2013; 43(1):15–27. http://dx.doi.org/10.1007/s00247-012-2496-x. [PubMed: 23288475]

Zanin E, Ranjeva J-P, Confort-Gouny S, Guye M, Denis D, Cozzone PJ, Girard N. White matter maturation of normal human fetal brain. an in vivo diffusion tensor tractography study: in vivo DTI tractography in human fetuses. Brain Behav. 2011; 1(2):95–108. http://dx.doi.org/10.1002/brb3.17. [PubMed: 22399089]

Zhang, Zhonghe; Liu, S.; Lin, X.; Teng, G.; Yu, T.; Fang, F.; Zang, F. Development of fetal brain of 20 weeks gestational age: assessment with post-mortem magnetic resonance imaging. Eur. J. Radiol. 2011; 80(3):e432–e439. http://dx.doi.org/10.1016/j.ejrad.2010.11.024. [PubMed: 21146341]

Zhang, Z.; Hou, Z.; Lin, X.; Teng, G.; Meng, H.; Zang, F.; Liu, S. Development of the fetal cerebral cortex in the second trimester: assessment with 7T postmortem MR imaging.. AJNR Am. J. Neuroradiol. 2013. http://dx.doi.org/10.3174/ajnr.A3406

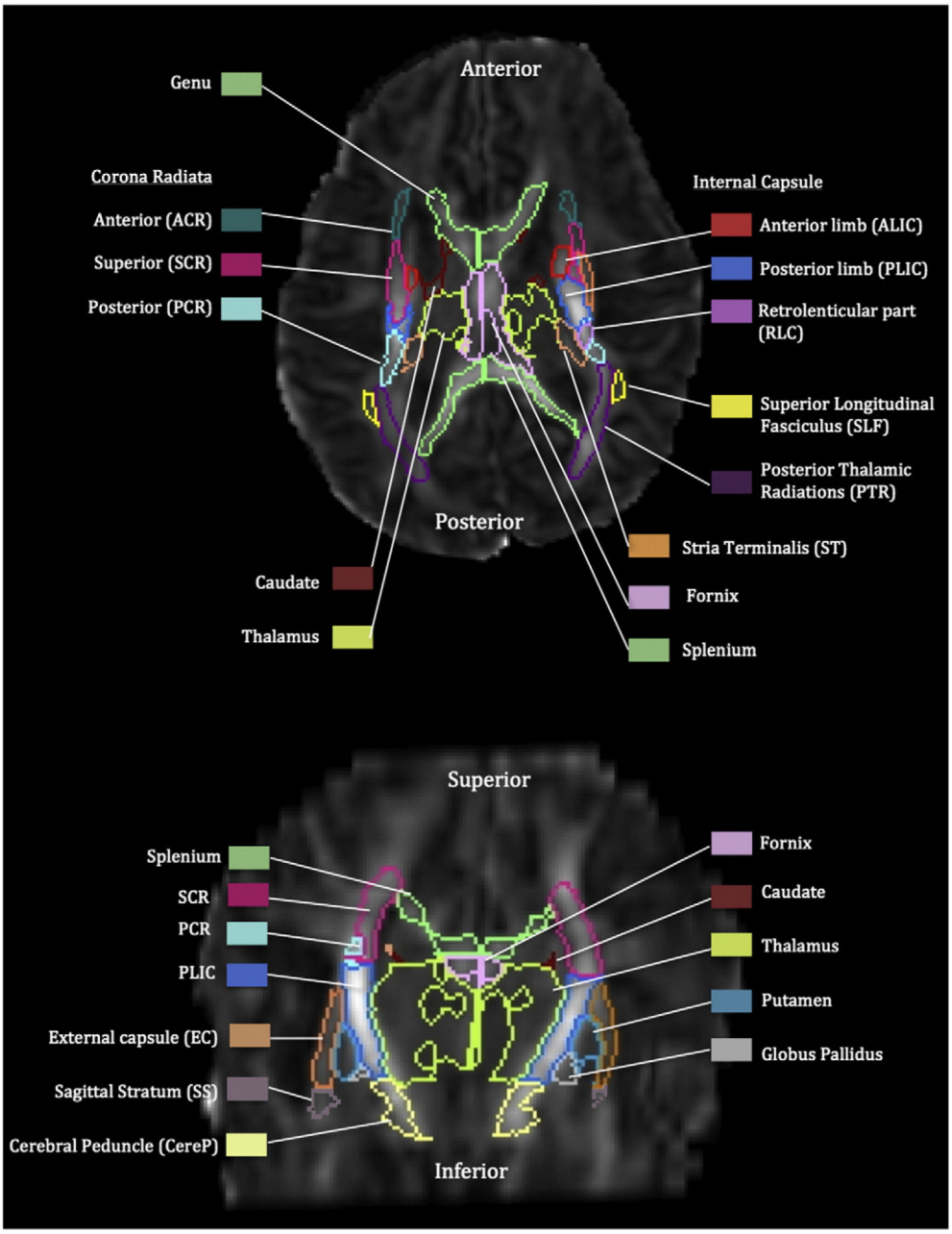

Fig. 1.

Brain regions selected on a representative infant DTI at near-term age using JHU DiffeoMap neonatal atlas for measurement of FA, MD, AD, and RD. (A = anterior, P = posterior).

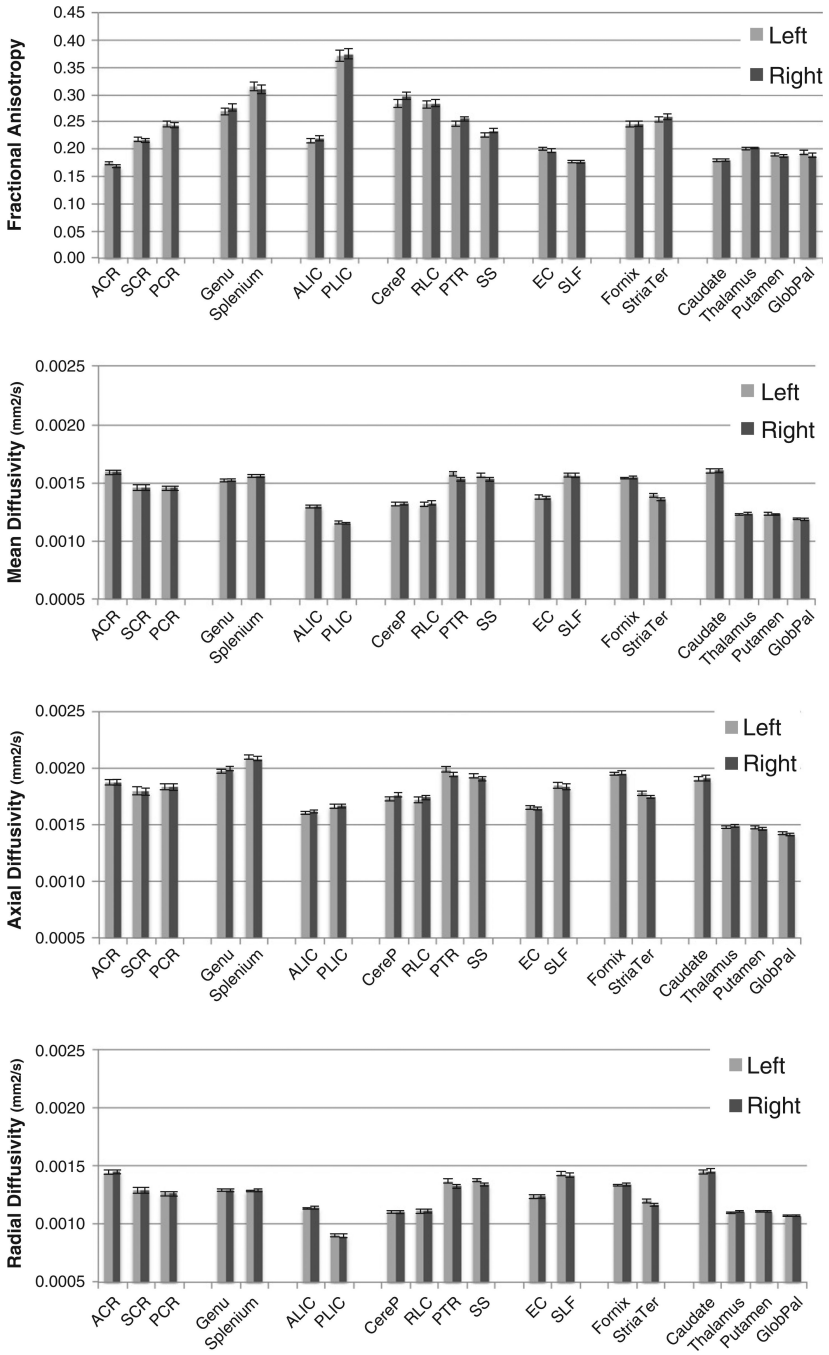

Fig. 2.

Brain regions assessed at near-term age with DTI measures of fractional anisotropy (FA), mean diffusivity (MD), axial diffusivity (AD), and radial diffusivity (RD) at near-term age (n = 45), mean (±95% CI).

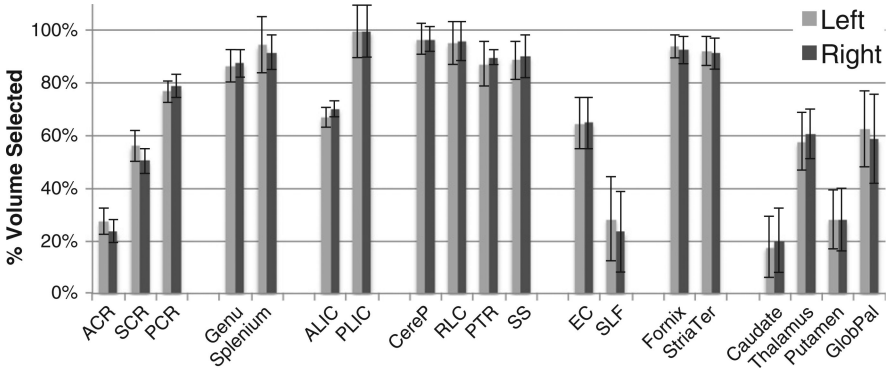

Fig. 3.

Near-term brain regional volumes selected using the threshold FA >0.15, reported as percent of total volume (mean ± 95%CI) of subcortical brain regions defined by the JHU neonatal atlas.

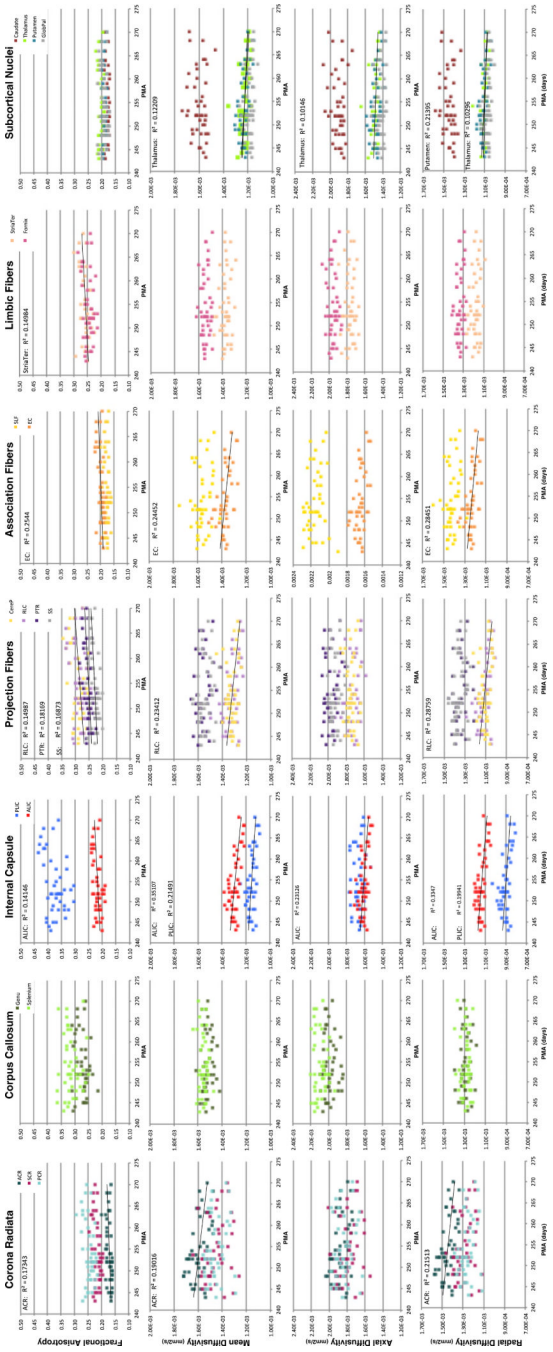

Fig. 4.

Near-term brain DTI values of fractional anisotropy (FA), mean diffusivity (MD), axial diffusivity (AD), and radial diffusivity (RD) in relation to PMA-at-scan (n = 45). Best-fit line and R^2 value noted for correlations with $p \leq 0.0125$.

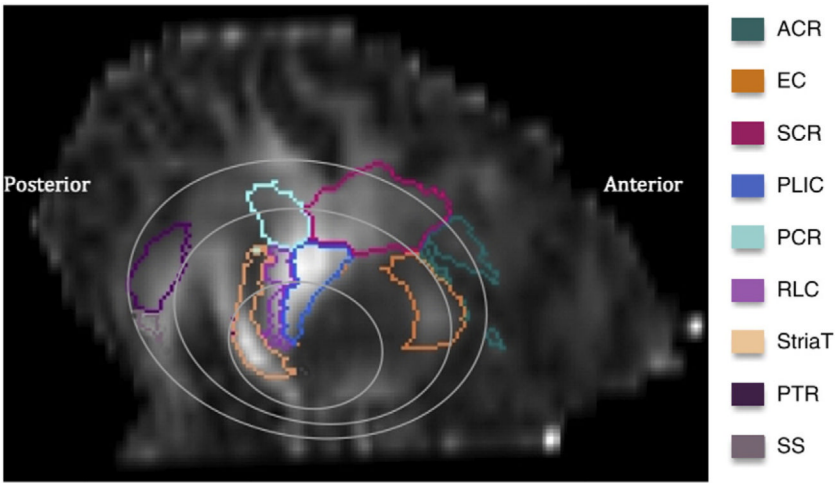

Fig. 5.

Near-term brain white matter regions selected on a representative infant DTI using JHU DiffeoMap neonatal atlas suggestive of central-to-peripheral temporal–spatial trajectories of WM microstructural development showing anterior corona radiata (ACR), superior corona radiata (SCR), posterior corona radiata (PCR), posterior limb of the internal capsule (PLIC), retrolenticular part of the internal capsule (RLC), posterior thalamic radiation (PTR), sagittal stratum (SS), external capsule (EC), and stria terminalis (StriaT).

Table 1

Participant demographics.

	All neonates	Neonates with DTI	Neonates with DTI, and normal MRI scanned at ≤40 weeks PMA
Total n=	**102**	**66**	**45**
Males/females, (%)	42/60 (41/59%)	25/41 (38/62%)	17/28 (38/62%)
Birth weight (g), mean (SD)	1087 (279)	1090 (266)	1092 (261)
GA-at-birth (weeks), mean (SD)	28.7 (2.4)	28.9 (2.3)	28.9 (2.3)
PMA-at-scan (weeks), mean (SD)	36.6 (l.8)	36.5 (1.3)	36.3 (1.0)
Maternal age (years), mean (SD)	31.6 (6.0)	31.9 (6.l)	32.3 (5.3)
Apgar at 5 min, mean (SD)	7.4 (1.8)	7.4 (1.7)	7.4 (1.7)
Bronchopulmonary dysplasia (%)	38 (37%)	25 (38%)	18 (40%)
Sepsis[b], (%)	19 (19%)	10 (15%)	7 (16%)
Necrotizing enterocolitis (%)	12 (12%)	8 (12%)	6 (13%)
Retinopathy of prematurity (%)	71 (70%)	46 (70%)	29 (64%)
Peak total bilirubin (mg/dL)[a] (SD)	7.9 (1.9)	7.8 (1.8)	7.6 (1.5)
Infants on mechanical vent (%)	64 (65%)	45 (68%)	30 (67%)

[a] Highest total serum bilirubin measurement during first two weeks of life.

[b] Sepsis with positive blood sample, as defined by the Neonatal Research Network

Table 2

Near-term brain region DTI parameters of FA, MD, AD, and RD for anterior (ACR), superior (SCR), and posterior (PCR) corona radiata, genu and splenium of the corpus callosum, anterior (ALIC) and posterior (PLIC) internal capsule, retrolenticular part of the internal capsule (RLC), posterior thalamic radiation (PTR), sagittal striatum (SS), external capsule (EC), superior longitudinal fasciculus (SLF), and mean ± 95% confidence intervals reported.

Regions	FA		Sig.	MD (×10E–3 mm^2/s)		Sig.	AD (×10E–3 mm^2/s)		Sig.	RD (×10E–3 mm^2/s)		Sig.
	Left	Right		Left	Right		Left	Right		Left	Right	
ACR	0.174 ± 0.003	0.168 ± 0.003	.000*	1.590 ± 0.022	1.592 ± 0.019	.000*	1.879 ± 0.026	1.874 ± 0.022	.000*	1.445 ± 0.020	1.451 ± 0.019	.000*
SCR	0.217 ± 0.004	0.216 ± 0.004	.000*	1.458 ± 0.028	1.455 ± 0.025	.564	1.801 ± 0.035	1.794 ± 0.031	.001*	1.287 ± 0.025	1.286 ± 0.023	.000*
PCR	0.246 ± 0.006	0.244 ± 0.005		1.452 ± 0.020	1.452 ± 0.022		1.838 ± 0.027	1.833 ± 0.029		1.259 ± 0.019	1.261 ± 0.020	
Genu	0.270 ± 0.007	0.276 ± 0.006	.000*	1.520 ± 0.012	1.525 ± 0.013	.000*	1.976 ± 0.020	1.993 ± 0.022	.000*	1.294 ± 0.013	1.290 ± 0.013	.512
Splenium	0.315 ± 0.009	0.309 ± 0.008		1.557 ± 0.010	1.556 ± 0.010		2.099 ± 0.022	2.086 ± 0.019		1.284 ± 0.012	1.290 ± 0.015	
ALIC	0.215 ± 0.005	0.220 ± 0.004	.000*	1.291 ± 0.012	1.296 ± 0.012	.000*	1.605 ± 0.015	1.618 ± 0.015	.000*	1.135 ± 0.012	1.137 ± 0.012	.000*
PLIC	0.371 ± 0.010	0.375 ± 0.010	.000*	1.156 ± 0.011	1.152 ± 0.010	.000*	1.663 ± 0.017	1.665 ± 0.016	.000*	0.904 ± 0.012	0.897 ± 0.013	.000*
RLC	0.282 ± 0.007	0.284 ± 0.007	.000*	1.313 ± 0.019	1.324 ± 0.017	.000*	1.718 ± 0.024	1.744 ± 0.022	.000*	1.110 ± 0.018	1.113 ± 0.018	.000*
PTR	0.247 ± 0.005	0.256 ± 0.005	.000*	1.577 ± 0.018	1.531 ± 0.018	.053	1.989 ± 0.022	1.944 ± 0.021	.000*	1.370 ± 0.018	1.324 ± 0.017	.030
SS	0.226 ± 0.005	0.233 ± 0.004		1.562 ± 0.015	1.528 ± 0.016		1.931 ± 0.016	1.910 ± 0.020		1.377 ± 0.016	1.338 ± 0.016	
EC	0.200 ± 0.003	0.197 ± 0.003	.000*	1.375 ± 0.016	1.371 ± 0.015	.000*	1.656 ± 0.019	1.642 ± 0.017	.000*	1.234 ± 0.016	1.235 ± 0.015	.000*
SLF	0.178 ± 0.003	0.176 ± 0.003		1.568 ± 0.019	1.559 ± 0.019		1.847 ± 0.023	1.833 ± 0.024		1.428 ± 0.018	1.420 ± 0.018	

*Significant differences in mean values between adjacent regions, $p \leq .003125$, corrected for multiple comparisons.

Table 3

Partial correlations (r) between near-term DTI values of fractional anisotropy (FA), mean diffusivity (MD), axial diffusivity (AD), and radial diffusivity (RD) with PMA-at-scan, controlling for GA-at-birth for brain regions: anterior (ACR), superior (SCR), and posterior (PCR) corona radiata, genu and splenium of the corpus callosum, anterior (ALIC) and posterior (PLIC) internal capsule, retrolenticular part of the internal capsule (RLC), posterior thalamic radiation (PTR), sagittal striatum (SS), external capsule (EC), superior longitudinal fasciculus (SLF), fornix, stria terminalis (StriaT), and subcortical nuclei

	FA Pearson's r	MD Pearson's r	AD Pearson's r	RD Pearson's r
ACR	.392, p = .009*	–.387, p = .009*	–.318, p = .035	–.418, p = .005*
SCR	.348, p = .021	–.182, p = .237	–.118, p = .444	–.220, p = .151
PCR	.320, p = .034	–.177, p = .251	–.089, p = .565	–.248, p = .105
Genu	.247, p = .106	–.041, p = .789	115, p = .456	–.121, p = .435
Splenium	.099, p = .522	.073, p = .636	.108, p = .484	.000, p = .999
ALIC	.433, p = .003*	–.545, p = .000**	–.411, p = .006*	–.540, p = .000**
PLIC	.352, p = .019	–.421, p = .004*	–.003, p = .986	–.436, p = .003*
CereP	.350, p = .020	–.164, p = .288	.030, p = .844	–.091, p = .556
RLC	.404, p = .007*	–.418, p = .005*	–.234, p = .127	–.485, p = .001**
PTR	390, p = .009*	–.175, p = .256	–.104, p = .503	–.217, p = .157
SS	.390, p = .009*	–.172, p = .265	–.072, p = .644	–.227, p = .139
EC	.477, p = .001**	–.424, p = .004*	–.327, p = .030	–.472, p = .001**
SLF	128, p = .407	–.203, p = .185	–.180, p = .241	–.222, p = .148
Fornix	230, p = .133	–.145, p = .348	.034, p = .826	–.234, p = .126
StriaT	.393, p = .008	–.237, p = .121	–.047, p = .764	–.285, p = .061
Caudate	–.160, p = .300	.108, p = .487	.112, p = .469	.151, p = .328
Thalamus	.170, p = .269	–.431, p = .003*	–.405, p = .006*	–.383, p = .010*
Putamen	.186, p = .226	–.361, p = .016	–.295, p = .052	–.395, p = .008*
Globus pallidus	.237, p = .122	–.210, p = .172	–.089, p = .564	–.274, p = .071

* $p \leq .0125$, corrected for multiple comparisons.

** $p \leq .001$.

Table 4

Partial correlations between near-term DTI values of fractional anisotropy (FA), mean diffusivity (MD), axial diffusivity (AD), and radial diffusivity (RD) with GA-at-birth, controlling for PMA-at-scan for brain regions: anterior (ACR), superior (SCR), and posterior (PCR) corona radiata, genu and splenium of the corpus callosum, anterior (ALIC) and posterior (PLIC) internal capsule, retrolenticular part of the internal capsule (RLC), posterior thalamic radiation (PTR), sagittal striatum (SS), external capsule (EC), superior longitudinal fasciculus (SLF), fornix, stria terminalis (StriaT), and subcortical nuclei.

	FA Pearson's r	MD Pearson's r	AD Pearson's r	RD Pearson's r
ACR	–.049, p = .754	.181, p = .239	.180, p = .243	.171, p = .266
SCR	–.033, p = .830	.221, p = .150	.220, p = .151	.208, p = .174
PCR	–.087, p = .576	.029, p = .852	.046, p = .766	–.001, p = .994
Genu	.267, p = .079	.155, p = .316	.343, p = .023	–.056, p = .718
Splenium	.235, p = .124	–.172, p = .264	.125, p = .420	–.280, p = .065
ALIC	.263, p = .085	.290, p = .056	.392, p = .008*	.167, p = .280
PLIC	.144, p = .351	.149, p = .335	.251, p = .101	–.020, p = .898
CereP	.015, p = .923	–.165, p = .285	–.122, p = .429	–.159, p = .302
RLC	.124, p = .423	.350, p = .020	.444, p = .003*	.256, p = .094
PTR	–.109, p = .480	–.032, p = .838	–.023, p = .882	–.018, p = .908
SS	–.031, p = .844	–.005, p = .976	.037, p = .814	–.031, p = .840
EC	–.062, p = .689	.443, p = .003*	.454, p = .002*	.415, p = .005*
SLF	–.009, p = .956	.005, p = .972	–.045, p = .770	.035, p = .823
Fornix	.123, p = .426	–.152, p = .324	–.060, p = .698	–.185, p = .229
StriaT	.083, p = .593	–.278, p = .067	–.213, p = .166	–.256, p = .094
Caudate	–.226, p = .140	.087, p = .575	.028, p = .855	.117, p = .451
Thalamus	–.009, p = .952	–.329, p = .029	–.334, p = .027	–.286, p = .060
Putamen	.166, p = .281	.374, p = .012*	.409, p = .006*	.315, p = .037
Globus pallidus	.240, p = .117	.127, p = .411	.185, p = .229	.057, p = .711

* $p \leq .0125$, corrected for multiple comparisons.

Table 5

Comparison of the order of regional FA values (from largest to smallest) and MD values (from smallest to largest) as measured in neonates (PMA 35–39 weeks) reported in the current study and previously reported in healthy infants (PMA 37–53 weeks) by Oishi et al. (2011).

Rose et al. (2013)	Mean FA	Oishi et. al (2011)	Mean FA		Rose et al. (2013)	Mean MD ($\times 10^{-3}$ mm^2/s)	Oishi et. al (2011)	Mean MD ($\times 10^{-3}$ mm^2/s)
PLIC	0.373	PLIC	0.410	More	PLIC	1.154	PLIC	1.057
CereP	0.290	CC	0.359	mature	Globus pallidus	1.187	Thalamus	1.100

Rose et al. (2013)	Mean FA	Oishi et. al (2011)	Mean FA		Rose et al. (2013)	Mean MD ($\times 10^{-3}$ mm^2/s)	Oishi et. al (2011)	Mean MD ($\times 10^{-3}$ mm^2/s)
RLC	0.283	CereP	0.342		Putamen	1.230	Globus pallidus	1.107
CC	0.265	RLC	0.336		Thalamus	1.230	Putamen	1.117
StriaT	0.257	Fornix	0.331		ALIC	1.294	ALIC	1.177
PTR	0.251	PCR	0.325		RLC	1.318	RLC	1.190
Fornix	0.246	StriaT	0.325		CereP	1.318	CereP	1.193
PCR	0.245	SCR	0.311		EC	1.373	EC	1.220
SS	0.229	PTR	0.307		StriaT	1.373	StriaT	1.247
ALIC	0.217	ALIC	0.304		PCR	1.452	Caudate	1.253
SCR	0.216	SS	0.294		SCR	1.457	PCR	1.313
Thalamus	0.202	EC	0.290		CC	1.540	Fomix	1.320
EC	0.198	SLF	0.278		Fornix	1.542	SCR	1.330

Rose et al. (2013)	**Mean FA**	**Oishi et. al (2011)**	**Mean FA**		**Rose et al. (2013)**	**Mean MD ($\times 10^{-3}$ mm^2/s)**	**Oishi et. al (2011)**	**Mean MD ($\times 10^{-3}$ mm^2/s)**
Globus pallidus	0.191	ACR	0.274	Less	SS	1.545	CC	1.383
Putamen	0.188	Thalamus	0.195	mature	PTR	1.554	PTR	1.383
Caudate	0.180	Globus pallidus	0.181		SLF	1.563	SS	1.397
SLF	0.177	Putamen	0.158		ACR	1.591	ACR	1.423
ACR	0.171	Caudate	0.142		Caudate	1.602	SLF	1.463